

UCSF

UC San Francisco Previously Published Works

Title

Radiosynthesis, ex Vivo Biodistribution, and in Vivo Positron Emission Tomography Imaging Evaluations of [¹¹C]2-Pyridinealdoxime Methiodide ([¹¹C]2-PAM): A First-In-Class Antidote Tracer for Organophosphate Intoxication.

Permalink

<https://escholarship.org/uc/item/69w4n4fm>

Journal

ACS Chemical Neuroscience, 9(12)

Authors

Neumann, Kiel
Blecha, Joseph
Hayes, Thomas
et al.

Publication Date

2018-12-19

DOI

10.1021/acscemneuro.8b00212

Peer reviewed



Published in final edited form as:

ACS Chem Neurosci. 2018 December 19; 9(12): 3007–3014. doi:10.1021/acschemneuro.8b00212.

Radiosynthesis, *ex Vivo* Biodistribution, and *in Vivo* Positron Emission Tomography Imaging Evaluations of [¹¹C]2-Pyridinealdoxime Methiodide ([¹¹C]2-PAM): A First-In-Class Antidote Tracer for Organophosphate Intoxication

Kiel D. Neumann[†], Joseph E. Blecha[†], Thomas R. Hayes[†], Tony Huynh[†], Chih-Kai Chao[‡], Nicolas Guilloteau[‡], Kurt R. Zinn[§], Henry F. VanBrocklin[†], Charles M. Thompson[‡], John M. Gerdes^{*,‡}

[†]Department of Radiology and Biomedical Imaging, University of California, San Francisco, San Francisco, California 94143, United States

[‡]Department of Biomedical and Pharmaceutical Sciences, University of Montana, Missoula, Montana 59812, United States

[§]Departments of Radiology and Biomedical Engineering, Michigan State University, East Lansing, Michigan 48824, United States

Abstract

2-Pyridinealdoxime methiodide (2-PAM) is a widely used antidote for the treatment of organophosphorus (OP) exposure that reactivates the target protein acetylcholinesterase. Carbon-11 2-PAM was prepared to more fully understand the *in vivo* mode of action, distribution, and dynamic qualities of this important countermeasure. Alkylation of 2-pyridinealdoxime with [¹¹C]CH₃I provided the first-in-class [¹¹C]2-PAM tracer in 3.5% decay corrected radiochemical yield from [¹¹C]CH₃I, >99% radiochemical purity, and 4831 Ci/mmol molar activity. [¹¹C]2-PAM tracer distribution was evaluated by *ex vivo* biodistribution and *in vivo* dynamic positron emission tomography (PET) imaging in naïve (OP exposure deficient) rats. Tracer alone and tracer coinjected with a body mass-scaled human therapeutic dose of 30 mg/kg nonradioactive 2-PAM demonstrated statistically similar tissue and blood distribution profiles with the greatest uptake in

*Corresponding Author: Phone: 406-243-4984; john.gerdes@umontana.edu.

Author Contributions

C.M.T. and J.M.G. designed the tracer. C.M.T. and N.G. performed the cold alkylation studies and prepared the nonradioactive tracer and metabolite standards. K.D.N., J.E.B., and H.F.V. developed the radiosynthesis. K.D.N., J.E.B., and T.R.H. produced [¹¹C]2-PAM and performed the rodent imaging, biodistribution studies, and blood metabolite analyses with T.H. C.-K.C. with J.M.G. performed the PET imaging analyses. J.M.G. and C.M.T. wrote the manuscript with contributions provided from C.-K. C., K.D.N., T.R.H., and H.V.B. All authors reviewed the manuscript.

Supporting Information

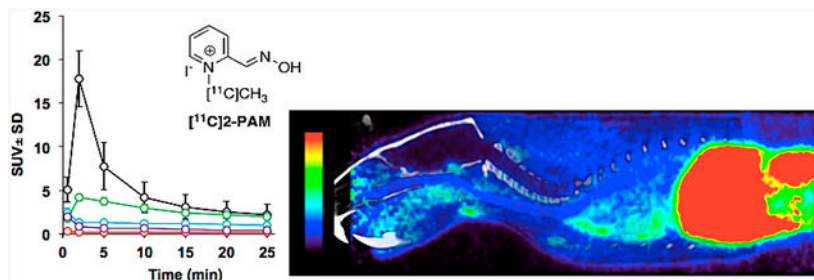
The Supporting Information is available free of charge on the ACS Publications website at DOI: 10.1021/acschemneur-o.8b00212. Chromatograms of the reversed-phase HPLC UV and radioactivity detection profiles of the semipreparative crude material tracer purification and similar analytical HPLC profiles; limited series of pyrido-2-aldoxime precursor, solvent (DMF, CH₃CN), temperature, and time radiolabeling trials reporting radiochemical yield and purity; enhanced views of the Figure 5, baseline (tracer alone), and tracer coinjected with 30 mg/kg cold 2-PAM, time–activity curves in rat; and numerical data from the baseline blood and brain tissue biodistribution experiments (Figure 2) (PDF)

Notes

The authors declare no competing financial interest.

kidney and significantly lower levels in liver, heart, and lung with lesser amounts in blood and brain. The imaging and biodistribution data show that radioactivity uptake in brain and peripheral organs is rapid and characterized by differential tissue radioactivity washout profiles. Analysis of arterial blood samples taken 5 min after injection showed ~82% parent [^{11}C]2-PAM tracer. The imaging and biodistribution data are now established, enabling future comparisons to outcomes acquired in OP intoxicated rodent models.

Graphical Abstract



Keywords

2-pyridinealdoxime methiodide (2-PAM); antidote; biodistribution; carbon-11; organophosphate; PET imaging

INTRODUCTION

The therapeutic agent 2-pyridinealdoxime methiodide (2-PAM, pralidoxime; Figure 1) is widely accepted as an antidote therapy in the United States (US) for the reactivation of acetylcholinesterase (AChE) that has been inhibited by organophosphorus compounds such as chemical warfare agents and certain insecticide oxons (Scheme 1).^{1–3} The combination of 2-PAM with other centrally acting drugs such as a muscarinic blocker (e.g., atropine⁴) and antiseizure medication (midazolam^{5,6}) along with other supportive regimens define the standard of care for OP exposures, including self-poisoning.⁷

The mechanism by which 2-PAM or P2S (the analogous methanesulfonate salt), in addition to other select oximes, regenerates acetylcholinesterase enzymatic activity occurs via nucleophilic displacement at the phosphorus atom of the serine-*O*-phosphoryl linkage (Scheme 1) by the oxime C=N–OH moiety. The charged pyridinium ring of 2-PAM plays a supportive role in this mechanism as it is believed to initially guide the antidote to the cation-attracting, peripheral binding domain of AChE and aids docking in the active site similar to that achieved by the natural substrate acetylcholine that also bears a quaternary amine. As an antidote therapeutic to OP intoxication, 2-PAM reacts selectively with OP-modified AChE and other OP-adducted esterases. In the absence of OP-AChE and esterase modifications, 2-PAM is without a specific high affinity *in vivo* target.

Despite the favorable role of the cation moiety in the enzyme activity restoration mechanism, it is believed that cationic 2-PAM is primarily distributed to peripheral tissues because the blood–brain barrier (BBB) impedes facile diffusion of the cationic antidote into

the central nervous system (CNS).^{8,9} Diminished CNS access by charged therapeutic agents such as 2-PAM limits their usefulness. However, select studies reported that 2-PAM does reactivate OP-modified AChE in rat brain.¹⁰ In support of that work, Sakurada and colleagues reported that 2-PAM enters rat brain in a dose-dependent manner in the absence of OP treatment using microdialysis measures.¹¹ Additionally, it has been shown that [¹⁴C]2-PAM enters brain more readily following exposure to the OP trichlofon (Dipterex; *O,O*-dimethyl, 2,2,2-trichloro-1-hydroxyethyl phosphonate).^{10,12} Although low concentrations of 2-PAM can enter the brain, it remains less clear how brain levels might vary over time within the first hour of 2-PAM administration, as a function of the absence or presence of OP exposure. In an effort to further interrogate 2-PAM brain penetration under these and related conditions, we sought to generate and initially evaluate carbon-11 ($t_{1/2} = 20.4$ min) radiolabeled 2-PAM ([¹¹C]2-PAM) tracer that would enable facile *ex vivo* and *in vivo* CNS and peripheral tissue determinations.

The [¹¹C]2-PAM tracer was considered ideal for preliminary assessments of pharmacokinetic (PK) properties in rat CNS and peripheral tissues by *ex vivo* biodistribution (bio-d) and *in vivo* positron emission tomography (PET) imaging evaluations. The acquired tracer data would ultimately enable correlation to previously established 2-PAM biochemical and toxicological study outcomes.^{1-3,7,11-14} In this study, we report the radiosynthesis of a first-in-class [¹¹C]2-PAM tracer and initial evaluations of the tracer using naïve rats that have not undergone OP exposure. The assessments include *ex vivo* bio-d measures, blood metabolite assessment, and *in vivo* PET imaging determinations after administration of tracer alone (baseline profiles). Additionally, we describe select experiments in which a therapeutic dose level of nonradioactive (cold) 2-PAM was coadministered with the tracer. Together, the naïve rat [¹¹C]2-PAM tracer profiles serve as fundamental data for comparisons to related future tracer measures in OP intoxicated rats.

RESULTS AND DISCUSSION

The high molar activity radiosynthesis of [¹¹C]2-PAM was developed based on literature precedent¹⁵ from the readily accessible radiolabeling synthon [¹¹C]methyl iodide ([¹¹C]-CH₃I)¹⁶ and 2-pyridinealdoxime, such that the tracer could be generated by a one-step alkylation procedure (Scheme 2). Special considerations were taken using the [¹¹C]CH₃I approach because most cold preparations of *N*-methylpyridinium ions use a large surplus of the alkyl iodide and long reaction times, relying on precipitation of the salt for isolation. Preliminary cold chemistry studies using a large inverse ratio of 10- to 50-fold 2-pyridinealdoxime relative to methyl iodide revealed that a high conversion (>80% based on methyl iodide as the limiting reagent) to 2-PAM could be accomplished in less than 5 min at 120 °C in dimethylformamide (DMF). Acetonitrile (CH₃CN) was also found as a suitable solvent and led to ~40% conversion to cold product under similar conditions. Methylation in other solvents such as DMSO, *N*-methylpyrrolidine, and dimethoxyethane (DME) were found to be less effective than DMF or CH₃CN when a surplus of 2-pyridinealdoxime was used. The nonradioactive reaction yield in either DMSO or CH₃CN was not improved at temperatures below 90 °C nor above 120 °C (sealed tube conditions).

Adaptation of the modified cold synthetic route to the corresponding radiosynthesis required [^{11}C]CH $_3$ I, which was prepared by an established gas-phase automated method.¹⁶ In this approach, [^{11}C]CH $_3$ I was bubbled into a solution of 2-pyridinealdoxime (1 mg) in CH $_3$ CN; the reaction vessel was sealed and heated at 120 °C for 8 min, then cooled briefly, diluted with saline, and the tracer was purified by reversed-phase high performance liquid chromatography (HPLC). The rapid formation of [^{11}C]2-PAM occurred in a decay-corrected radiochemical yield of $3.5 \pm 0.9\%$ ($n = 8$), relative to [^{11}C]CH $_3$ I with a measured molar activity of $4,831 \pm 911$ Ci/mmol ($n = 8$), >99% radiochemical purity, and in a total synthesis time of 40 min from delivery of [^{11}C]CH $_3$ I. A similar protocol using DMF as the reaction solvent at 140 °C afforded a higher decay-corrected tracer yield ($16.5 \pm 6.5\%$, $n = 3$) relative to [^{11}C]CH $_3$ I; yet, purification by HPLC was difficult when DMF was used as reaction solvent, resulting in a lower tracer radiochemical purity (85–90%, see: Supporting Information). A limited series of reactions was conducted in an attempt to increase the yield of [^{11}C]2-PAM using CH $_3$ CN as the reaction solvent. Adjusting temperature (80–120°C) and mass of precursor (5–10 mg) did not afford an improved yield of [^{11}C]2-PAM (per Supporting Information, Additional Labeling Studies for [^{11}C]2-PAM Preparation, Table S1). Because the use of CH $_3$ CN solvent was superior for gaining higher final tracer purity, albeit affording tracer in lower radiochemical yield, the CH $_3$ CN protocol was used for the reported preclinical studies. Tracer doses, formulated in ~1 mL sterile isotonic saline, were found to be stable for >2 h at room temperature by HPLC analysis, and up to 10 mCi (nondecay corrected) of final formulated [^{11}C]2-PAM tracer was typically achieved.

To initially appraise CNS and peripheral tissue tracer uptake profiles, bio-d determinations and PET imaging studies were performed using 250–400 g (mean body weight 305 g) male Sprague–Dawley rats ($n = 3$ per group) that were administered [^{11}C]2-PAM by tail vein intravenous (i.v.) injection under light isoflurane (1–2%) anesthesia. Biodistribution experiments used 100–200 μCi tracer doses (1.0–1.5 mL) where the initial studies were carried out with tracer alone (baseline conditions). Baseline *ex vivo* biodistribution radioactivity profiles (blood and tissues) were sampled at select 2–60 min time points after tracer injection (Figure 2) for blood, brain, liver, heart, kidney, and bone (femur). The samples were counted affording data as decay-corrected percent injected dose radioactivity per gram tissue values (% ID/g) \pm standard error measures (SEM). The bio-d radioactivity profiles reveal highest uptake in kidney with significantly diminished amounts in liver, lower uptake in lung and heart, and the lowest radioactivity in blood, brain, and bone. For all samples, time-dependent radioactivity uptake and washout profiles were observed for the tissues and blood over 60 min. The rapid radioactivity uptake and washout seen within naïve rat tissues (i.e., lack of an OP-AChE modification) are consistent with the absence of a high affinity 2-PAM target within the tissues and blood.

The elevated radioactivity in kidney at 2 and 5 min was anticipated for a cationic, highly water-soluble compound and thought to be associated with clearance.^{17,18} Limited brain radioactivity uptake observed at all times is considered to be a function of the diminished ability of cationic [^{11}C]2-PAM (and/or related species) to diffuse across the BBB.^{11,12} Applying the average-sized rat brain blood volume of ~30–35 $\mu\text{L/g}$ of tissue¹⁹ for the blood and brain % injected dose (ID) per gram profiles over time (Figure 2) indicates that ~8–15% of the brain radioactivity detected over the 2–60 min is contributed from the cerebral blood

pool radioactivity within brain tissue. Thus, the majority of the brain radioactivity (Figure 2) is associated with tissue (see Methods section and Supporting Information).

Tracer metabolism events are thought to contribute to the liver radioactivity levels (Figure 2).^{12,20} Because the highest liver radioactivity was observed at 5 min, evaluation of blood nonprotein-bound fraction components was conducted to assess the amount of parent tracer activity relative to metabolites. Tail artery blood sampling at 5 min, blood sample processing and chromatographic profiling against nonradioactive (cold) chemical metabolite standards afforded a distribution of radioactivity components (Figure 3). At 5 min after tracer injection, the nonprotein-bound fraction showed 82.3% parent [¹¹C]2-PAM tracer and a mixture of metabolites, including 4.4% *N*-methyl-2-pyridinecarboxaldehyde, 4.7% of a mixture of *N*-methyl-2-pyridinecarboxamide, *N*-methyl-2-pyridinecarboxylic acid, *N*-methyl-2-pyridinecarbonitrile, and 8.6% *N*-methyl-2-pyridone (Figure 3). The metabolite structures and relative distribution are consistent with 2-PAM metabolites reported previously,^{12,15,20} albeit with some minor differences that could result from dose sizes and rat strains. The Figure 3 metabolism results provide insight into the maximal 5 min liver bio-d profile. At present, it remains unclear whether uptake of the metabolites into brain occurs, if are produced in brain, or both.

We sought to further interrogate the 5 min bio-d time point because previous studies with 2-PAM have shown a dose-dependent increase in brain penetration.¹¹ Our initial appraisal used tracer that was coinjected with a 30 mg/kg of cold 2-PAM dose that is akin to a human 30 mg/kg therapeutic 2-PAM dose,^{1,3,11} where the total mass of cold 2-PAM injected was not allometrically scaled. The experiment was designed to compare the presence versus absence of cold 2-PAM in relation to activity uptake and washout profiles in naïve rats in the absence of an OP-AChE modification. Further, differential tracer tissue interactions associated with metabolism, clearance or other processes might also be detected in the presence of cold therapeutic agent. The results are shown in Figure 4 with baseline (tracer alone) versus 30 mg/kg cold 2-PAM dose coinjected with tracer. One-way ANOVA analyses show no significant differences between the two tracer dose regimens, [¹¹C]2-PAM only (baseline) versus tracer in the presence of 30 mg/kg cold 2-PAM, in most of tissue activity distributions at 5 min except the liver ($P = 0.0085$). The significant elevated liver activity in the presence of cold 2-PAM is thought to be a result of altered tracer metabolic processes. No significant difference in 2-PAM brain radioactivity uptake between tracer alone and tracer plus therapeutic cold 2-PAM dose experiments was found, suggesting that the uptake was not affected by mass dose level. With the exception of liver and in the absence of OP-AChE modification, the naïve rat activity biodistribution PK profiles resulting from [¹¹C]2-PAM tracer low mass doses (Figure 4) are thought to be similar to those of higher mass doses of nonradioactive 2-PAM.^{17,18}

To distinguish the *in vivo* radioactivity tissue distributions in naïve rats, 30 min dynamic *in vivo* PET scanning (5 min frames) was employed that used 0.5–1.0 mCi tracer i.v. doses. The 30 min scan time was based on the rapid radioactivity uptake and washout defined by the bio-d profiles (Figure 2). The PET scans were carried out to afford *in vivo* data for comparison to the *ex vivo* biodistribution profiles. The PET imaging was carried out in parallel with microcomputed axial tomography (CT) and magnetic resonance (MR) scanning

for the sake of anatomical tissue information and data coregistration allowing for conservatively defined volumetric three-dimensional regions of interest (ROIs) relative to established rat brain and peripheral tissue atlas designations.^{21–23} Regional radioactivity signals were determined as standardized uptake values (SUV, see Methods section)²⁴ that permitted imaging evaluations across rats for determinations of the mean ($n = 3$) SUV values \pm SD per ROI vs time (min). The resultant tracer baseline and tracer in the presence of cold 2-PAM time–activity curves (Figure 5) and expanded the brain TAC data (Figure 6) were obtained. A typical sagittal PET view of summed radioactivity coregistered with CT data after baseline [¹¹C]2-PAM tracer injection is depicted in Figure 7.

Baseline PET imaging TAC plots (Figure 5, Panel A) show high radioactivity in kidney, less in liver, low levels in heart and lung, and lower level activity in whole brain. These relative *in vivo* SUV profiles are similar to the *ex vivo* biodistribution radioactivity determinations (Figure 2). An analogous assessment was made when [¹¹C]2-PAM was coinjected with 30 mg/kg of cold 2-PAM (Figure 5, Panel B) showing the similarity (Panel A vs Panel B) and significant amounts of radioactivity washout by 25 min after tracer injection. The relative distributed amounts of radioactivity detected (Figure 5, Panel A and B) are found similar to the *ex vivo* bio-d profiles of Figure 2; that is, radioactivity distribution profiles as kidney \gg liver > heart, lung > brain. The elevated radioactivity found in kidney and liver as compared to heart and lung (Figure 5) likely represents greater tissue reservoirs for 2-PAM (and related radiolabeled species) associated with clearance and metabolism, respectively. The Figure 5 mean radioactivity liver values at 5 min after tracer injection do not clearly show a distinction between the Panel A (tracer alone) vs Panel B (tracer in the presence of 30 mg/kg cold 2-PAM), whereas differences are found from the similar liver bio-d determinations as shown in Figure 4. The reasons for the differences remain unclear. The expanded naïve rat brain TAC plots (Figure 6) for baseline and the coinjection of cold 2-PAM experiments reveal that the curves are not significantly different from each other. Radioactivity enters the brain rapidly, albeit at low levels, and reaches a steady concentration in the brain after 5 min. Low brain radioactivity uptake was anticipated based on previous biodistribution reports using naïve rats.^{11,12}

The PET imaging results demonstrate that the use of the short carbon-11 half-life [¹¹C]2-PAM tracer within naïve rats is suitable for quantitatively detecting radioactivity PK uptake and washout changes in tissues of interest. The baseline PET data reveals radioactivity distributions that are relatively uniform relative to the *ex vivo* time–radioactivity biodistribution determinations. Within naïve rat tissues, the PET TAC data from the coinjection of nonradioactive 2-PAM is similar to those from baseline profiles, which we consider consistent for the naïve rat condition that is devoid of an OP-AChE adduct (Scheme 1), and lacks a high affinity 2-PAM target.

CONCLUSIONS

To gain deeper insights into the pharmacokinetic properties of the therapeutic antidote 2-PAM, the first-in-class [¹¹C]2-PAM tracer was selected for study initially within naïve (OP exposure deficient) rats that lack a high affinity *in vivo* target for the tracer. The tracer was prepared by a straightforward approach using a one-step alkylation reaction with [¹¹C]CH₃I

followed by HPLC purification, providing stable (2 h) saline-formulated dose preparations that were administered intravenously. Initial uptake and washout radioactivity PK assessments within CNS and peripheral tissues, and also blood, were made by *ex vivo* biodistribution profiling over 60 min. Radioactivity distributions were realized for baseline (tracer alone) and at the selected 5 min time with tracer coinjected with cold 2-PAM (human therapeutic dose level, 30 mg/kg). A range of high to low radioactivity was found in blood and tissues; respectively, kidney >> liver > lung and heart >> blood, brain and bone. The high kidney radioactivity was anticipated for a water-soluble cationic compound, and similarly, the low brain activity was expected based on the diminished ability of cationic species to diffuse across the BBB. Realizing the liver activity maxima at 5 min could be related to previously described 2-PAM metabolic transformations and that this activity level was affected by cold 2-PAM coadministration, arterial blood collection under baseline conditions at 5 min and subsequent processing revealed plasma free-fraction activity components as 82.3% parent [¹¹C]2-PAM tracer and just 17.7% as cognate metabolites previously described in the literature.

Dynamic *in vivo* PET imaging for 30 min using [¹¹C]2-PAM tracer under baseline conditions and also tracer coinjected with 30 mg/kg cold 2-PAM revealed CNS and peripheral tissue radioactivity distributions that were relatively similar to the time–radioactivity profiles established by the *ex vivo* biodistribution experiments. The nonradioactive 2-PAM plus tracer conditions were found without significant differences on brain radioactivity profiles over 30 min, which was expected for naïve rats that lack a high-affinity OP-AChE adduct target. The PET imaging confirms low radioactivity uptake into brain as previously described in the literature for nonradioactive 2-PAM. In summary, the naïve rat *ex vivo* biodistribution and *in vivo* PET imaging time–radioactivity measures after [¹¹C]2-PAM tracer i.v. injection serve as fundamental correlated data sets. This requisite data is now poised to enable meaningful comparisons relative to tracer determinations in OP-intoxicated rats in which the detection of [¹¹C]2-PAM participation in the critical therapeutic regeneration of acetylcholinesterase activity will be probed.

METHODS

General.

Reagents (e.g., 2-pyridinealdoxime, iodomethane, etc.) and solvents such as anhydrous dimethylformamide (DMF), anhydrous acetonitrile (CH₃CN), and 2-pyridinealdoxime methiodide were reagent grade or better, used without any additional purification, and were purchased from Sigma-Aldrich Chemical Co. (Milwaukee, WI). USP-grade sterile isotonic saline was also purchased from Sigma-Aldrich. 2-Pyridinecarboxaldehyde, 2-pyridinecarboxamide, 2-pyridinecarboxylic acid, and 2-pyridinecarbonitrile were converted into the *N*-methyl pyridinium metabolite standards per literature methods.^{25,26} Nuclear magnetic resonance (NMR) data were recorded in CDCl₃ on a Varian Avance 400 MHz spectrometer. High performance liquid chromatography (HPLC) was performed with a Waters 590 system (Milford, MA) coupled to a Shimadzu SPD UV–visible detector (Columbia, MD) and a gamma counting in-line radiation flow detector (Model 105s, CRA; Berkeley, CA). The HPLC data was collected with a SRI Peaksimple, model 304, data

system (Torrance, CA). Counting of tissue and blood samples utilized a Hidex automated gamma counter (Turku, Finland).

Male Sprague–Dawley rats (250–400 g; Charles River, Inc., Skokie, IL) were used for the [^{11}C]2-PAM biodistribution, blood, and PET imaging studies. The animals were cared for and used at the University of California, San Francisco (UCSF) facilities that are accredited by the American Association for Accreditation of Laboratory Animal Care (AAALAC). The animal studies adhered to UCSF IACUC approved protocols that satisfied NIH guidelines and institutional regulations. Prior to injection of [^{11}C]2-PAM, rats were lightly anesthetized (~1–2% isoflurane), and lateral tail vein catheters were installed in the lower tail portion. The catheter line was flushed with 200 μL of saline and capped. Thereafter, the catheter cap was removed, tracer was injected as a bolus, and then the catheter was flushed with 0.3 mL saline.

Synthesis of 2-PAM under Limiting Methyl Iodide Reagent Conditions.

2-Pyridinealdoxime (10 mg; 0.082 mmol) was dissolved in 200 μL of DMF at 125 °C or CH_3CN at 80 °C and added dropwise to a solution of methyl iodide (2.0 μL) in 50 μL of DMF or CH_3CN over 5 min. After the addition, the reaction was kept at the indicated temperature for 5 min. The percent conversion to 2-PAM was 80–90% (DMF) and 35–40% (CH_3CN) as determined by NMR integration of aldoxime $\text{CH}=\text{N}$ peaks or by the ratio of the $\text{N}-\text{CH}_3$ to aromatic region in d_6 -DMSO. Conversion to 2-PAM in CH_3CN was $40 \pm 4\%$ (using 2-PAM as internal standard) as measured by reversed-phase HPLC (UV at 290 nm) following evaporation of the solvent *in vacuo*, using a Sonoma C₁₈(2) 5 μ 100 Å 15 cm \times 4.6 mm (ES Industries; West Berlin, NJ) column with a mobile phase of 10% $\text{C}_2\text{H}_5\text{OH}/10 \text{ mM}$ 2-(*N*-morpholino)ethanesulfonic acid in H_2O at 1.0 mL/min.

Radiosynthesis of [^{11}C]2-PAM.

2-Pyridinealdoxime (1–10 mg) was dissolved in 300 μL of anhydrous CH_3CN in a 4 mL 1-dram vial and sealed with a Teflon-lined silicone septum screw-cap. Utilizing a gas-phase method¹⁶ and a GE Tracerlab FX C Pro radiosynthesis box, [^{11}C] CH_3I was produced and then bubbled into the CH_3CN solution, and the reactor vial was sealed. The mixture was heated at 80–140 °C for 8 min on an aluminum block heater. The reactor vial was removed from the heating source and allowed to cool for 60 s. The cap was removed; the CH_3CN solution was diluted with 2.5 mL of saline, and the crude material was injected onto a 10 \times 250 mm, 10 μm Hamilton PRP-1 HPLC column. The HPLC purification used saline as mobile phase at a flow rate of 3 mL/min with a retention time of [^{11}C]2-PAM at 8.5 min (see Supporting Information, Chromatograms section for representative HPLC elution profiles, and the Additional Radiolabeling Studies for [^{11}C]2-PAM Production section).

Dose Formulation.

Doses of [^{11}C]2PAM were formulated in sterile isotonic saline (pH ~ 7) as 100–200 μCi in 1.0–1.5 mL for the biodistribution and blood determinations, and also 0.5–1.0 mCi in 0.5–1.0 mL for the PET imaging evaluations; in which the average dose volume across both sets of experiments was ~1.0 mL. Before animal dosing, quality control of the dosing was accomplished by analytical HPLC (7 μm Hamilton PRP-1 4.6 \times 250 mm flow rate 1 mL/

min) demonstrating >99% radiochemical purity and >95% chemical purity. In separate experiments, doses were allowed to remain at room temperature for 2 h and then subjected to reversed-phase analytical HPLC analysis (see Supporting Information).

Rat Biodistribution Studies.

Rats received a bolus injection of 100–200 μCi of [^{11}C]2-PAM via tail vein catheter port followed by a 0.3 mL saline flush. Rats were euthanized by lateral chest puncture under anesthesia and dissected at 2, 5, 10, 30, and 60 min after injection ($n = 3$ per time point). Blood was collected by cardiac puncture immediately prior to euthanasia at each time point. Whole organs of brain, liver, heart, kidneys, lungs, bone (femur), and blood were collected into 20 mL preweighed glass scintillation vials and capped, where they were placed into a Hidex automated gamma counter (Hidex AMG) to be counted and weighed. Decay corrected data was exported from the Hidex instrument to Excel (Microsoft Office) software and plotted as decay corrected percent injected dose per gram (% ID/g) \pm SEM versus time (min). To compare the % ID/g values of the two tracer dose regimens (i.e., tracer alone and tracer in the presence of 30 mg/kg of cold 2-PAM) one-way ANOVA analyses were performed for each tissue and blood using R software (version 3.0 or later).

Calculated Estimates of Blood Activity in Biodistribution Rat Brain Tissues.

Rat blood and brain tissue biodistribution radioactivity data from 2 to 60 min were analyzed to estimate the amount of the percent contribution of blood signal in brain tissue. Everett¹⁹ previously reported that average-sized rat brain blood volume is $\sim 30\text{--}35 \mu\text{L/g}$ of tissue. Using a midrange brain blood volume of $32.5 \mu\text{L/g}$ (equal to 0.0325 mL/g), and blood and brain % ID/g values per time point (Figure 2; per Supporting Information, Numerical Blood and Brain Data) with a blood density of 1 g/mL afforded the following relationships (eqs 1 and 2) and ratio (eq 3), where $t =$ time point measured (for example at t_1):

$$\text{blood at } t_1 (\% \text{ID/g}) = \text{blood } \% \text{ID/g at } t_1 \times 1 \text{ g/1 mL} \times 0.0325 \text{ mL/g} \quad (1)$$

$$\text{brain at } t_1 (\% \text{ID/g}) = \text{brain } \% \text{ID/g at } t_1 \quad (2)$$

$$\% \text{ of blood in brain tissue at } t_1 (\% \text{ID/g}) = \text{blood at } t_1 (\% \text{ID/g}) / \text{brain at } t_1 (\% \text{ID/g}) \times 100 \quad (3)$$

Rat Arterial Blood Metabolites.

Rats were installed with a tail artery catheter at the upper tail region for blood sampling, and the catheter was flushed with saline heparin solution prior to blood collection. Tracer (1–3 mCi) was injected via a lower tail vein catheter, and then 5 min later arterial blood ($100 \mu\text{L}$) was collected by heparin treated syringe. Blood samples were placed in heparin treated plastic 1.5 mL snap-lid vials containing $10 \mu\text{L}$ of 10 mg/mL citric acid and centrifuged at $13\ 200 \text{ g}$ for 1 min, and remaining supernatant was removed and placed in a second tube. The

supernatant was treated with 100 μL of acetonitrile to precipitate protein; the protein pellet was removed after centrifugation, and the serum supernatant was collected. Chromatographic separation of serum radioactive components was conducted by preparative thin layer chromatography (TLC, 3.5×10 cm aluminum-backed silica with fluorescent indicator (254 nm), mobile phase = *n*-butanol:acetic acid:water (5:1:3)) to accommodate the carbon-11 half-life. The chromatography was run in parallel with known cold chemical metabolite standards^{12,15,20} that were prepared in-house by literature methods.^{25,26} Co-migration of standards with radioactive spots were excised with scissors, placed in 20 mL glass scintillation vials, and counted with the Hidex gamma counter. The data were exported from the Hidex instrument to Excel software and reported as relative % of total radioactivity, defined as the decay corrected ratio of component radioactivity over the sum of all radioactivity counted across the samples $\times 100$.

Rat PET-CT and MR Imaging Studies.

Tracer [¹¹C]2-PAM i.v. bolus doses of 0.5–2.0 mCi as formulated in 0.5–2.0 mL of saline were administered. The cold 2-PAM PET imaging experiments were accomplished by coinjecting 2-PAM at 30 mg/kg, saline (1–2 mL) with tracer. The PET, CT, and MR imaging were performed normothermic (37 °C) under isoflurane anesthesia (1–1.5%). The PET and CT imaging data were acquired with a Siemens Inveon microPET/CT scanner system (ca. 1.5 mm PET imaging spatial resolution). Dynamic PET imaging data were acquired over 30 min beginning ~0.5 min after the time of injection of tracer. The PET data were reconstructed with using a Siemens Inveon reconstruction program suite, including OSEM2D; as 6 frames, 300 s per frame for the 30 min scans, decay time corrected, and quantified with a radiation phantom instrument calibration factor. A partial volume correction was not applied, and conservative ROI definitions were used as described below. The CT data were acquired in standard rat mode: 80 kVp, 225 mA; 400 ms exposure, 194 steps \times 194 degrees, and 97- μm isotropic resolution. The MR data were acquired with a Bruker Biospin 7-T magnet using a multislice 2D FLASH protocol with the following parameters: T2*-weighted gradient recall echo, TR = 1528.3 ms, TE = 7 ms, and $256 \times 256 \times 50$ voxels, affording $16 \mu\text{m}^3$ resolution.

The reconstructed MR, CT, and PET imaging data files were processed with AMIDE open source software²⁷ (SourceForge), version 1.0.4 (or later versions). The MR and CT images were oriented as defined by Paxinos^{21,22} and Walker.²³ Cranial landmarks of bregma and lambda were identified from the CT images. The *x*, *y*, and *z* coordinates of imaging views were centered at bregma, equivalent to the origin of the first scan, and then consistent landmark structures were iteratively coregistered and template fit against the cranial structures of the first scan landmarks. Subsequently, the landmarks were correlated with cerebral soft tissues from the MR scans.

The coregistered imaging data permitted ROIs (Figures 5–7) to be defined within their ROI volume size limits and locations and against established stereotaxic three-dimensional locations.^{21–23} The ROIs were defined as follows: whole brain, heart, lung, kidney, and liver. PET scan regional tissue radioactivity is reported as Standardized Uptake Value (SUV) defined as [activity concentration in the tissue region of interest (MBq/cc)/decay corrected injected dose at time = 0 (MBq)] \times body weight of the rat as gram (g).²⁴ ROI PET scan

statistics (SUV \pm SD) collected from time points at midframe were exported to Excel, and plots of SUV versus time were generated using either Excel or GraphPad Prism (La Jolla, CA) software.

Supplementary Material

Refer to Web version on PubMed Central for supplementary material.

ACKNOWLEDGMENTS

We are grateful for support from the NIH and the expert radiochemical technical assistance of Ms. Salma Jivan of the Department of Radiology and Biomedical Imaging at the University of California, San Francisco.

Funding

Research reported in this publication was supported by the National Institute of Neurological Disorders and Stroke of the National Institutes of Health under Award U01NS092495. The content is solely the responsibility of the authors and does not necessarily represent the official views of the National Institutes of Health.

ABBREVIATIONS

ACh	acetylcholine
AChE	acetylcholinesterase
ANOVA	analysis of variance
bio-d	biodistribution
BBB	blood–brain barrier
CH₃CN	acetonitrile
CNS	central nervous system
CT	microcomputed axial tomography
DMF	dimethylformamide
DMSO	dimethyl sulfoxide
HPLC	reversed-phase high performance liquid chromatography
ID	injected dose
i.v.	intravenous
MR	magnetic resonance
min	minutes
NMR	nuclear magnetic resonance
2-PAM	2-pyridinealdoxime methiodide
P2S	2-pyridinealdoxime methylmethanesulfonate

PET	positron emission tomography
PK	pharmacokinetic
OP	organophosphate
OP-AChE adduct	phosphorylated acetylcholinesterase
RCY	radiochemical yield
ROI	region of interest
SD	standard deviation
SEM	standard error measures
SUV	standardized uptake value
TAC	time–activity curve
TLC	thin-layer chromatography
UV	ultra-violet

REFERENCES

- (1). Jokanovic M (2012) Structure-activity relationship and efficacy of pyridinium oximes in the treatment of poisoning with organo-phosphorus compounds: a review of recent data. *Curr. Top. Med. Chem* 12, 1775–1789. [PubMed: 23030612]
- (2). Jokanovic M, and Prostran M (2009) Pyridinium oximes as cholinesterase reactivators. Structure-activity relationship and efficacy in the treatment of poisoning with organophosphorus compounds. *Curr. Med. Chem* 16, 2177–2188. [PubMed: 19519385]
- (3). Jokanovic M, and Stojiljkovic MP (2006) Current understanding of the application of pyridinium oximes as cholinesterase reactivators in treatment of organophosphate poisoning. *Eur. J. Pharmacol* 553, 10–17. [PubMed: 17109842]
- (4). Shih TM, and McDonough JH Jr. (1999) Organo-phosphorus nerve agents-induced seizures and efficacy of atropine sulfate as anticonvulsant treatment. *Pharmacol. Biochem. Behav* 64, 147–153. [PubMed: 10495009]
- (5). Gilat E, Goldman M, Lahat E, Levy A, Rabinovitz I, Cohen G, Brandeis R, Amitai G, Alkalai D, and Eshel G (2003) Nasal midazolam as a novel anticonvulsive treatment against organo-phosphate-induced seizure activity in the guinea pig. *Arch. Toxicol* 77, 167–172. [PubMed: 12632257]
- (6). Reddy SD, and Reddy DS (2015) Midazolam as an anticonvulsant antidote for organophosphate intoxication-A pharma-cotherapeutic appraisal. *Epilepsia* 56, 813–821. [PubMed: 26032507]
- (7). Eddleston M, Buckley NA, Eyer P, and Dawson AH (2008) Management of acute organophosphorus pesticide poisoning. *Lancet* 371, 597–607. [PubMed: 17706760]
- (8). Bodor N, Shek E, and Higuchi T (1976) Improved delivery through biological membranes. 1. Synthesis and properties of 1-methyl-1,6-dihydropyridine-2-carbaldoxime, a pro-drug of N-methyl-pyridinium-2-carbaldoxime chloride. *J. Med. Chem* 19, 102–107. [PubMed: 1246030]
- (9). Bodor N, Shek E, and Higuchi T (1975) Delivery of a quaternary pyridinium salt across the blood–brain barrier by its dihydropyridine derivative. *Science* 190, 155–156. [PubMed: 1166305]
- (10). Hobbiger F, and Vojvodic V (1967) The reactivation by pyridium aldoximes of phosphorylated acetylcholinesterase in the central nervous system. *Biochem. Pharmacol* 16, 455–462. [PubMed: 6034365]

- (11). Sakurada K, Matsubara K, Shimizu K, Shiono H, Seto Y, Tsuge K, Yoshino M, Sakai I, Mukoyama H, and Takatori T (2003) Pralidoxime Iodide (2-PAM) Penetrates across the Blood-Brain Barrier. *Neurochem. Res* 28, 1401–1407. [PubMed: 12938863]
- (12). Firemark H, Barlow CF, and Roth LJ (1964) The Penetration of 2-Pam-C14 into Brain and the Effect of Cholinesterase Inhibitors on Its Transport. *J. Pharmacol. Exp. Ther* 145, 252–265. [PubMed: 14214425]
- (13). Petrikovics I, Papahadjopoulos D, Hong K, Cheng TC, Baskin SI, Jiang J, Jaszberenyi JC, Logue BA, Szilasi M, McGuinn WD, and Way JL (2004) Comparing therapeutic and prophylactic protection against the lethal effect of paraoxon. *Toxicol. Sci* 77, 258–262. [PubMed: 12857941]
- (14). Shih TM, Skovira JW, O'Donnell JC, and McDonough JH (2010) In vivo reactivation by oximes of inhibited blood, brain and peripheral tissue cholinesterase activity following exposure to nerve agents in guinea pigs. *Chem.-Biol. Interact* 187, 207–214. [PubMed: 20223229]
- (15). Poziomek EJ, Hackley BE, and Steinberg GM (1958) Pyridinium Aldoximes 1. *J. Org. Chem* 23, 714–717.
- (16). Larsen P, Ulin J, Dahlström K, and Jensen M (1997) Synthesis of [¹¹C]iodomethane by iodination of [¹¹C]methane. *Appl. Radiat. Isot* 48, 153–157.
- (17). Jovanovic D (1989) Pharmacokinetics of pralidoxime chloride. A comparative study in healthy volunteers and in organophosphorus poisoning. *Arch. Toxicol* 63, 416–418. [PubMed: 2818204]
- (18). Gupta RC (2015) *Handbook of Toxicology of Chemical Warfare Agents*, 2nd ed., Elsevier/AP, Amsterdam/Boston.
- (19). Everett NB, Simmons B, and Lasher EP (1956) Distribution of blood (Fe 59) and plasma (I 131) volumes of rats determined by liquid nitrogen freezing. *Circ. Res* 4, 419–424. [PubMed: 13330185]
- (20). Enander I, Sundwall A, and Sorbo B (1962) Metabolic studies on N-methylpyridinium-2-aldoxime. III. Experiments with the ¹⁴C-labelled compound. *Biochem. Pharmacol* 11, 377–382. [PubMed: 13890155]
- (21). Paxinos G (2015) Preface. In *The Rat Nervous System*, 4th ed., p xi, Academic Press, San Diego.
- (22). Paxinos G, and Watson C (2007) *The Rat Brain in Stereotaxic Coordinates*, 6th ed., Academic Press/Elsevier, Amsterdam/Boston.
- (23). Walker WFH, and Dominique G (1997) *Anatomy and Dissection of the Rat*, 3rd ed., Freeman, W. H. & Company, New York.
- (24). Gambhir SS (2004) Quantitative Assay Development for PET In *Molecular Imaging and its Biological Applications* (Phelps ME., Ed.), pp 130–132, Springer, New York, NY.
- (25). Ellin RI (1958) Stability of Pyridine-2-aldoxime Methiodide. I. Mechanism of Breakdown in Aqueous Alkaline Solution. *J. Am. Chem. Soc* 80, 6588–6590.
- (26). Ellin RI, Carlese JS, and Kondritzer AA (1962) Stability of pyridine-2-aldoxime methiodide II. Kinetics of deterioration in dilute aqueous solutions. *J. Pharm. Sci* 51, 141–146. [PubMed: 13889913]
- (27). Loening AM, and Gambhir SS (2003) AMIDE: a free software tool for multimodality medical image analysis. *Mol. Imaging* 2, 131–137. [PubMed: 14649056]

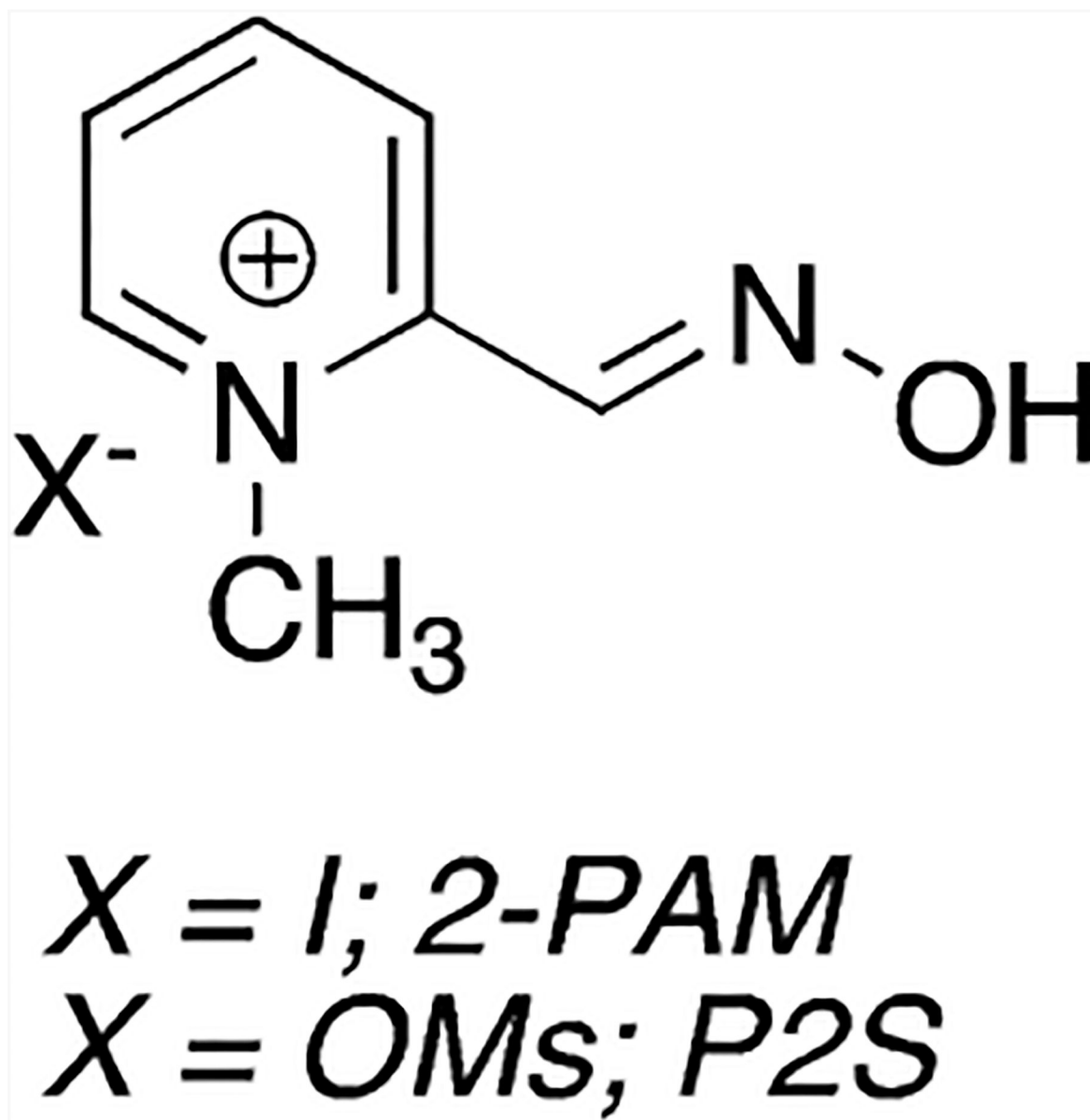


Figure 1.
Chemical structures of the pyridine aldoximes.

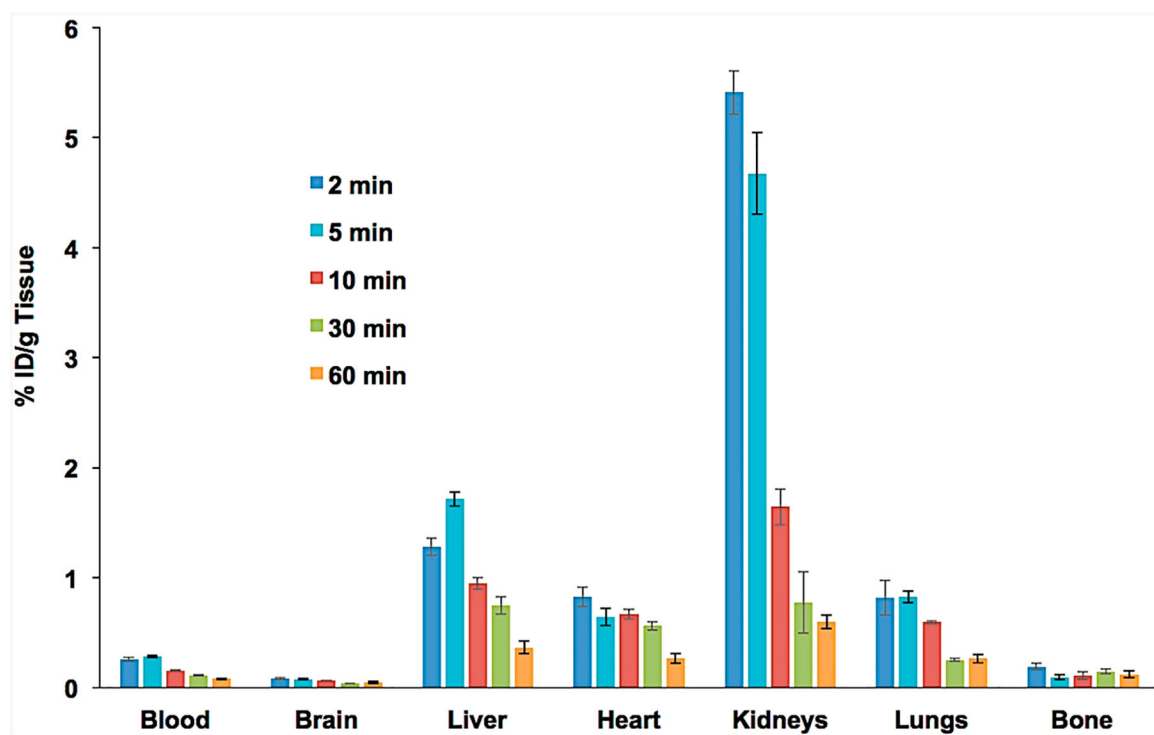


Figure 2. Mean baseline (tracer alone, $n = 3$, \pm SEM) biodistribution (2–60 min) of decay-corrected radioactivity after [^{11}C]2-PAM tracer i.v. injection in naïve rats.

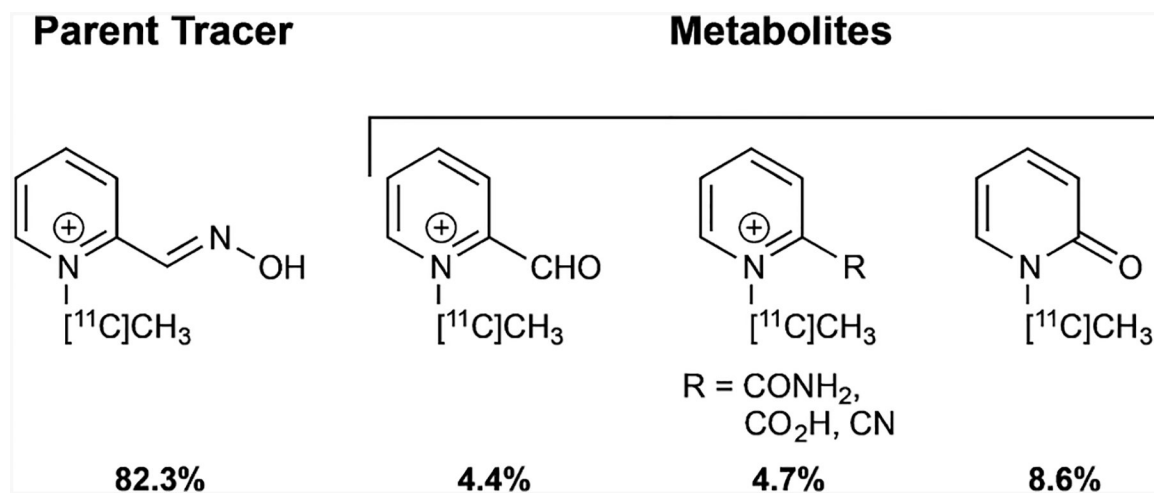


Figure 3. Plasma free-fraction relative radioactive components determined by chromatographic separation and counting at 5 min after tracer injection.

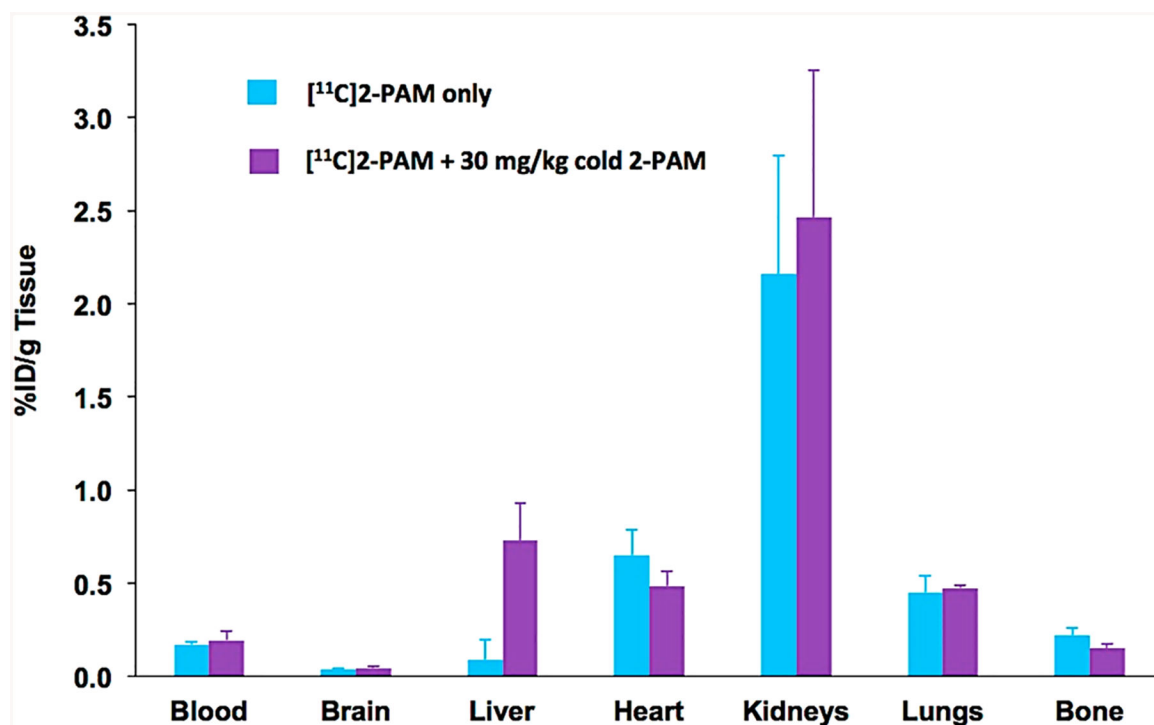


Figure 4. Comparison of the mean ($n = 3$, \pm SEM) radioactivity (decay-corrected) biodistributions of baseline [¹¹C]2-PAM (tracer alone, aqua) and [¹¹C]2-PAM coinjected with 30 mg/kg cold 2-PAM (purple) at 5 min after respective tracer i.v. injections in naïve rats.

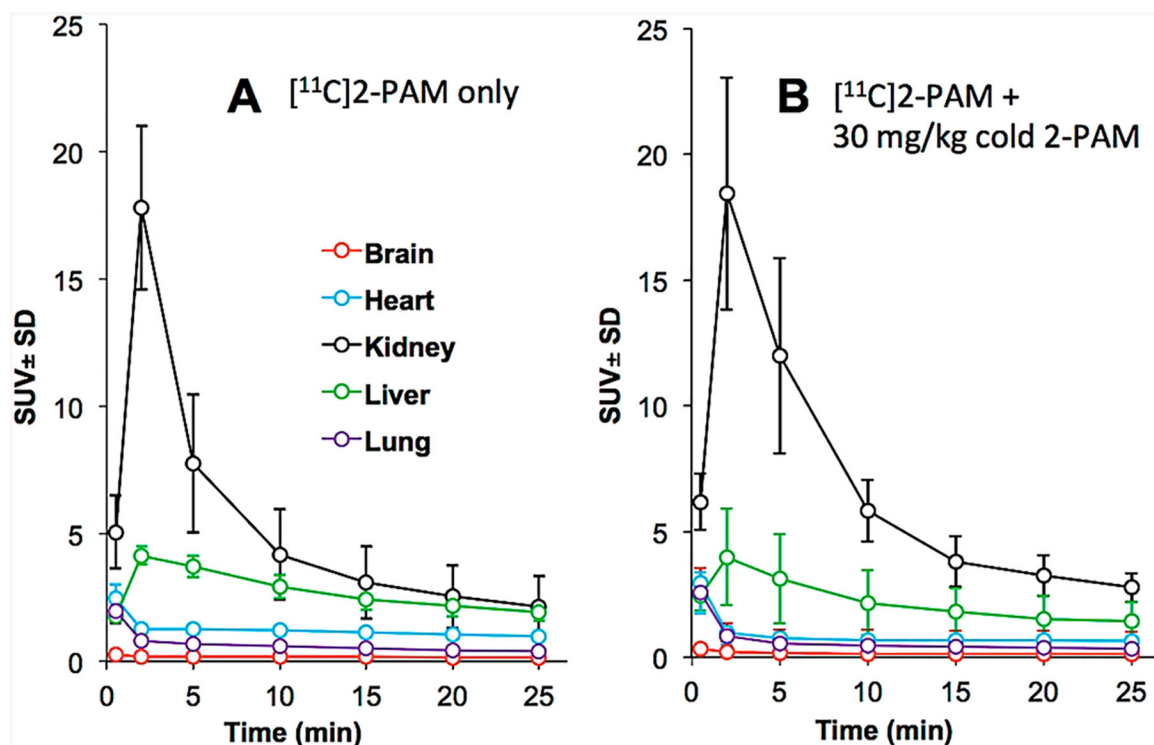


Figure 5. Mean values ($n = 3$, \pm SD) PET imaging detected radioactivity (decay corrected and subject normalized as SUV) vs time (min) curves in naïve rats after [¹¹C]2-PAM tracer: Panel A, tracer alone (baseline) and Panel B, tracer coinjected with 30 mg/kg cold 2-PAM (see Supporting Information for expanded plots of these curves).

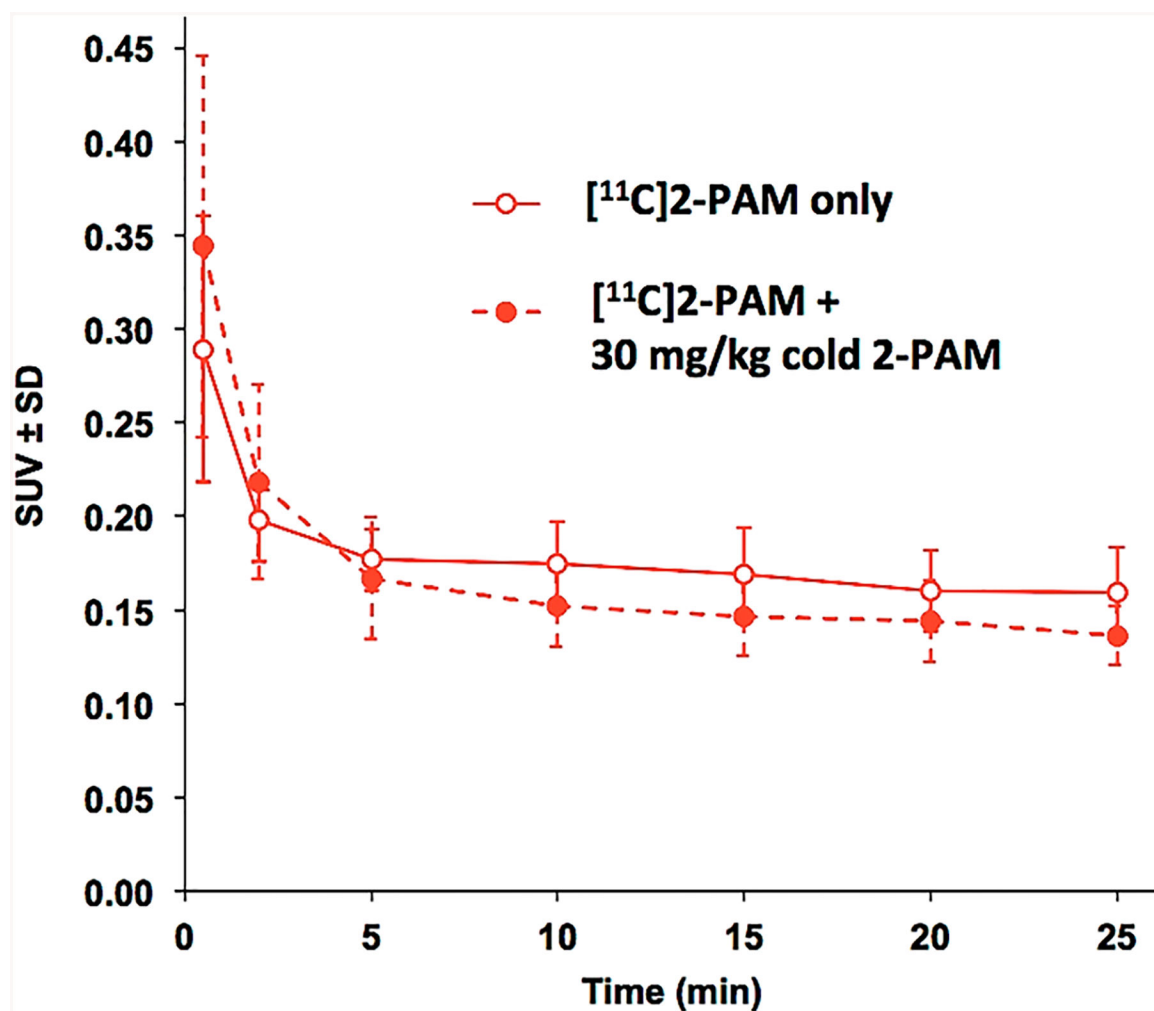


Figure 6. Expanded view PET imaging brain time–activity curves of mean SUV ($n = 3, \pm$ SD) vs time (min) for [¹¹C]2-PAM tracer alone (baseline; open circles and solid line) and tracer coinjected with 30 mg/kg cold 2-PAM (solid points and dashed line).

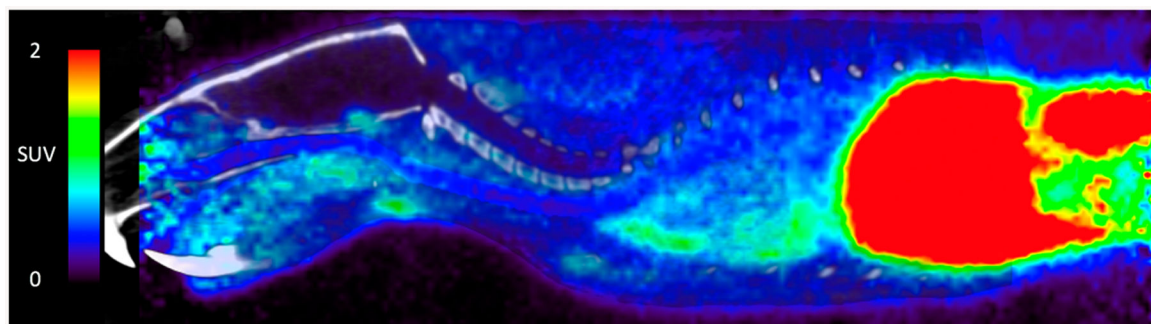
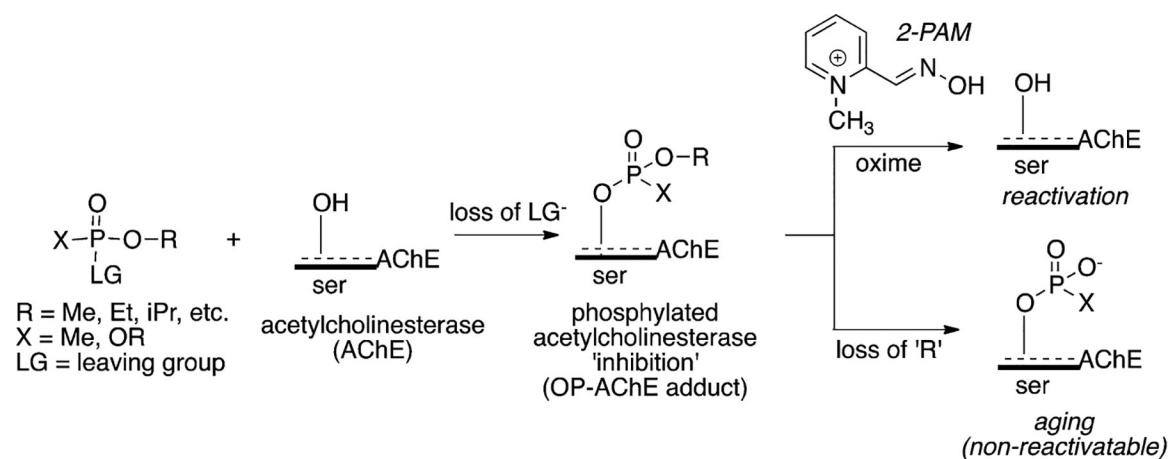
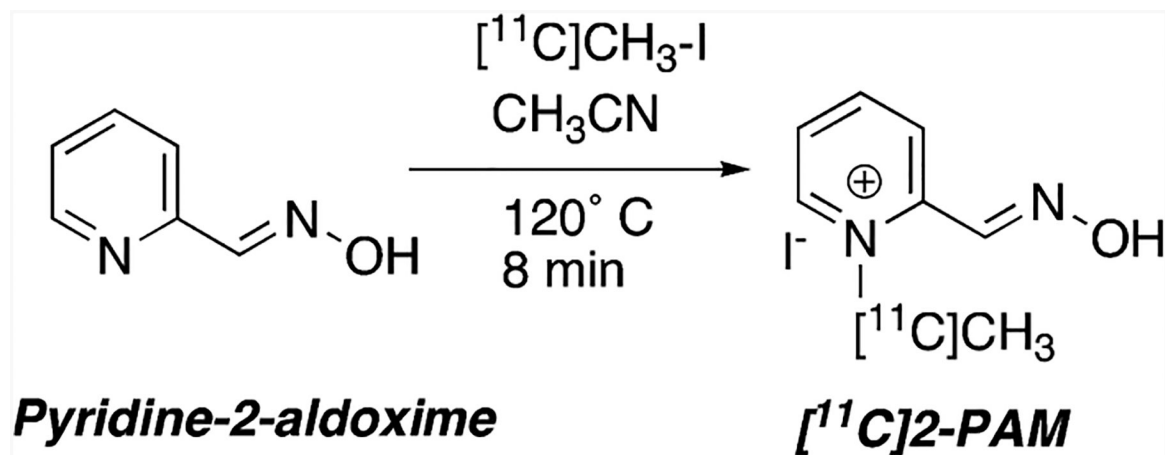


Figure 7. A PET-CT sagittal (cranial, rostral left; caudal right) view near midline (MR data omitted for clarity) of 30 min summed activity (SUV color bar) after injection of 0.95 mCi of [^{11}C]2-PAM tracer alone (baseline) in a male 330 g rat.



Scheme 1.
 Inhibition of Acetylcholinesterase by Organophosphorus Compounds and Reactivation of the OP-AChE Adduct by 2-PAM



Scheme 2.
Radiosynthesis of Tracer [C^{11}]2-PAM